# Spectroscopic and Computational Investigation of the H155A Variant of Cysteine Dioxygenase: Geometric and Electronic Consequences of a Third-Sphere Amino Acid Substitution

Elizabeth J. Blaesi,[†,§] Brian G. Fox,[‡] and Thomas C. Brunold*,[†]

[†]Department of Chemistry, University of Wisconsin—Madison, Madison, Wisconsin 53706, United States
[‡]Department of Biochemistry, University of Wisconsin—Madison, Madison, Wisconsin 53706, United States

Ⓢ Supporting Information

**ABSTRACT:** Cysteine dioxygenase (CDO) is a mononuclear, non-heme iron(II)-dependent enzyme that utilizes molecular oxygen to catalyze the oxidation of L-cysteine (Cys) to cysteinesulfinic acid. Although the kinetic consequences of various outer-sphere amino acid substitutions have previously been assessed, the effects of these substitutions on the geometric and electronic structures of the active site remained largely unexplored. In this work, we have performed a spectroscopic and computational characterization of the H155A CDO variant, which was previously shown to display a rate of Cys oxidation ~100-fold decreased relative to that of wild-type (WT) CDO. Magnetic circular dichroism and electron paramagnetic resonance spectroscopic data indicate that the His155 → Ala substitution has a significant effect on the electronic structure of the Cys-bound Fe(II)CDO active site. An analysis of these data within the framework of density functional theory calculations reveals that Cys-bound H155A Fe(II)CDO possesses a six-coordinate Fe(II) center, differing from the analogous WT CDO species in the presence of an additional water ligand. The enhanced affinity of the Cys-bound Fe(II) center for a sixth ligand in the H155A CDO variant likely stems from the increased level of conformational freedom of the cysteine–tyrosine cross-link in the absence of the H155 imidazole ring. Notably, the nitrosyl adduct of Cys-bound Fe(II)CDO [which mimics the (O₂/Cys)–CDO intermediate] is essentially unaffected by the H155A substitution, suggesting that the primary role played by the H155 side chain in CDO catalysis is to discourage the binding of a water molecule to the Cys-bound Fe(II)CDO active site.
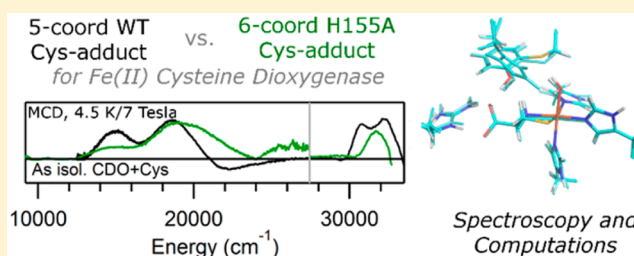
Cysteine dioxygenase (CDO) is a mononuclear, non-heme iron enzyme that catalyzes the oxidation of exogenous cysteine (Cys) by $O_2$ to cysteinesulfinic acid with nearly complete substrate fidelity.[1−3] This conversion represents the only oxidative degradation pathway for Cys,[4] and it has been proposed that CDO is ultimately responsible for the majority of taurine produced in mammals.[5] Malfunctioning CDO has been implicated in a variety of neurological disorders, such as Alzheimer's, Parkinson's, and motor neuron diseases.[6−10] Additionally, recent studies have shown that the *CDO1* gene is downregulated through the methylation of its promoter in certain forms of human cancers (including breast and colorectal), and that tumor growth may be suppressed through the restoration of the normal levels of *CDO1* expression.[11,12]

The first CDO crystal structure (published in 2006[13]) revealed several unique geometric features of this enzyme, including an intramolecular cross-link between residues C93 and Y157, as well as a rare three-histidine (3His) facial ligation sphere about the iron center in the resting state of the enzyme. Subsequent crystal structures have provided evidence of bidentate binding of the substrate Cys through its thiolate and amino groups,[14] and a direct Fe−S bonding interaction [or Fe−Se interaction in the case of CDO incubated with the substrate analogue selenocysteine (Sec)] was confirmed

through resonance Raman and magnetic circular dichroism (MCD) spectroscopic studies.[15] Recent work by our group has suggested that although Cys-bound Fe(II)CDO features a five-coordinate active site (as previously revealed by multiple X-ray crystal structures[14,16]), the Fe center of Cys-bound Fe(III)-CDO additionally possesses a hydroxide ligand to adopt a six-coordinate, distorted octahedral coordination environment.[17]

In an effort to obtain molecular-level insight into the CDO reaction mechanism, analogues for dioxygen (including NO, CN⁻, and superoxide) have been used with great success to mimic catalytically relevant species. The first major spectroscopic investigation of CDO revealed that the nitrosyl adduct of Cys-bound Fe(II)CDO represents a rare $S = \frac{1}{2}$ {FeNO}⁷ species, as opposed to an $S = \frac{3}{2}$ species as is typically observed for non-heme iron enzymes.[18] A subsequent spectroscopic and computational study of this unusual {FeNO}⁷ species revealed that the presence of a strongly π-donating thiolate ligand and the neutral 3His facial ligation to the Fe center are key contributors to the stabilization of the $S = \frac{1}{2}$ state [where a

low-spin Fe(II) ion is ligated by an NO•] over the $S = {}^{3}/_{2}$ state [featuring a high-spin Fe(III) ion coupled antiferromagnetically to NO⁻]. The spectroscopically validated computational methodology developed in this work was then used to propose a mechanism for $O_2$ activation by CDO in which the iron oxidation state never exceeds +3 and the substrate Cys acts as a redox non-innocent ligand.[19] In support of this proposal, subsequent experimental and computational studies revealed that the same computational methodology could be used successfully to describe the geometric and electronic properties of the different species formed upon incubation of CDO with azide, superoxide, and cyanide.[3,17,20]

Although the kinetic consequences of substituting various outer-sphere residues on the catalytic properties of CDO have been assessed in several studies,[3,16,21] in all but one case these variants have not yet been characterized spectroscopically to probe their perturbed geometric and electronic active site structures.[3] To overcome these deficiencies, we have initiated combined spectroscopic and computational studies of CDO variants for identifying specific roles performed by individual outer-sphere residues in the catalytic cycle. In this study, the H155 residue was replaced with an alanine to examine how the imidazole side chain influences the properties of the CDO active site and its interaction with the Cys and $O_2$ substrates.

Residue H155 is a member of the S153−H155−Y157 (mouse CDO numbering) catalytic triad motif that is highly conserved among CDO enzymes. The presence of this motif has been successfully used to screen protein sequences to identify members of the cupin superfamily with CDO activity, including several previously unknown bacterial homologues.[22] X-ray crystallographic data of Cys-bound CDO revealed these three residues engage in an extended hydrogen bonding network, with the oxygen atom of the S153 side chain residing within 2.65 Å of the Nε atom of H155, and the Nδ atom of H155 located 2.77 Å from the Y157 oxygen atom (see Figure 1).[14] As the Y157 phenol is in turn located within hydrogen
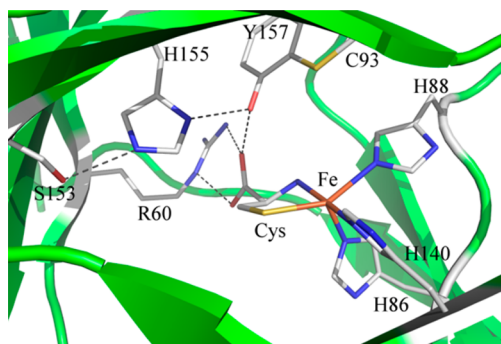


**Figure 1.** Crystal structure of Cys-bound Fe(II)CDO from rat (Protein Data Bank entry 4JTO, 2.00 Å resolution).[14] Potential hydrogen bonds are shown as dashed lines.

bonding distance of the carboxylic acid group of the substrate Cys, the interactions between H155 and neighboring residues may exert significant control over the positioning of the Cys substrate at the active site. Additionally, H155 is one of the few acidic active site residues available to act as a proton donor and may thus be involved in the putative proton transfer to an intermediate that occurs between $O_2$ activation and product release.[23] Consistent with these predictions, it was found that the specific activity of the H155A CDO variant is significantly lower ($k_{cat} < 0.1$ s⁻¹) than that of the wild-type (WT) enzyme

($k_{cat} = 8.6$ s⁻¹).[3] Moreover, a $K_M$ for binding of Cys to the variant enzyme could not be determined as no saturation was observed even at 25 mM Cys.[3]

## ■ EXPERIMENTAL PROCEDURES

**Gene Expression and Protein Purification.** The wild-type (WT) CDO gene from *Mus musculus* was cloned into a pVP16 vector with maltose binding protein (MBP) as an N-terminal fusion protein tag, as previously described.[13] To generate the H155A mutant plasmid DNA, polymerase chain reaction (PCR) was performed with a Herculase II kit on the WT CDO-containing vector, using forward and reverse mutagenic primers (25 nucleotides in length, with the mutated codon centered in the primer sequences) where the nucleotides describing the H155 codon were substituted appropriately to create the H155A mutant plasmid DNA. The resultant DNA was treated with the DpnI restriction enzyme for 1 h at 37 °C to destroy the original WT CDO DNA template. Competent JM109 cells were exposed to the mutant plasmid, heat shocked, and plated onto a lysogeny broth/agar medium containing ampicillin (to which the pVP16 plasmid confers resistance). Individual bacterial colonies that resulted from this process were separately grown further in 10 mL cultures overnight at 37 °C. The plasmid DNA from the cells in each culture was isolated by use of a QIAprep kit and sequenced using a Big Dye kit in conjunction with the Sanger sequencing method (at the University of Wisconsin—Madison Biotechnology Center) to ensure the mutagenesis was both successful and selective for the desired mutation. Plasmids with alternative, extra, or no mutations were discarded.

Expression from the H155A plasmid and purification of the corresponding H155A protein variant were conducted in the same manner as for the WT version of this protein, which has been described elsewhere.[19] In brief, CDO was expressed in *Escherichia coli* BL21(DE3) cells through induction with isopropyl β-D-1-thiogalactopyranoside (IPTG). The protein purification was conducted through the use of pulsed sonication cell disruption and three separatory columns, namely, diethylaminoethyl (DEAE) cellulose anion exchange, amylose affinity (to bind the fusion protein exclusively), and size-exclusion (Sephacryl S-100) columns. After elution from the amylose column, but before application to the S-100 column, fractions containing the MBP−CDO fusion protein were incubated overnight with tobacco etch virus protease to release the MBP affinity tag from the target CDO protein.

Similar to the WT enzyme,[18] H155A CDO was isolated with iron occupying only a fraction of active sites (∼20%) and with an Fe(II):Fe(III) ratio of ∼45:55. The activity of the as-isolated H155A CDO variant was verified by use of a qualitative thin-layer chromatography-based assay, as described elsewhere (Figure S1 of the Supporting Information).[15] It has been shown previously that the fraction of CDO protein molecules containing of the C93−Y157 thioether cross-link can be estimated on the basis of the double-band pattern observed on a sodium dodecyl sulfate−polyacrylamide gel electrophoresis (SDS−PAGE) gel.[24] Although a gel previously published by Pierce and co-workers did not exhibit the lower band associated with cross-linked H155A CDO,[3] in our hands a portion of the as-isolated variant clearly contains this C−Y cross-link, albeit in a yield somewhat lower than that of the WT protein (see Figure S2 of the Supporting Information). However, because cross-linked CDO is more stable than protein lacking the cross-link[21] and cross-link formation requires the presence of iron at the

active site,[25] it is reasonable to assume that the majority of iron-bound active sites in our H155A CDO samples were in the cross-linked form.

**Sample Preparation.** The iron(II) and iron(III) content of the protein was determined through a colorimetric assay using the iron chelator tripyridyl triazine (TPTZ) and an $\varepsilon_{590}$ of 22.1 mM$^{-1}$ cm$^{-1}$.[26] The assay was performed in the presence and absence of a reductant (hydroxylamine) to determine the proportion of Fe(II) versus Fe(III) initially present. As neither the variant nor WT CDO protein had iron bound at all active sites, the concentration of protein cited herein refers to the Fe-bound fraction, not that of the total protein. Samples used for spectroscopy were prepared anaerobically via either Schlenk line or glovebox methods and contained a 5-fold excess of L-cysteine (Cys) or L-selenocysteine (Sec) over Fe-bound CDO. Sec was prepared through the anaerobic reduction of selenocystine with tris(2-carboxyethyl)phosphine (TCEP). The nitrosyl adducts of Cys- or Sec-bound Fe(II)CDO were prepared through the introduction of NO gas (generated through the anaerobic reaction of aqueous cupric chloride, sodium nitrite, and ascorbic acid) to the sample vial headspace, as described previously.[19] Where applicable, sodium azide was added in a 200-fold molar excess over Fe-bound CDO. Samples for low-temperature (LT) Abs and MCD studies also contained 55% (v/v) glycerol as a glassing agent.

**Spectroscopy.** Room-temperature absorption (RT Abs) spectra were obtained using a Varian Cary 5e spectrophotometer, while the sample compartment was purged with N$_2$(g). LT Abs and MCD spectra were recorded with a Jasco J-715 spectropolarimeter in conjunction with an Oxford Instruments SM4000-8T magnetocryostat. The MCD spectra presented herein were recorded by taking the difference between the spectra obtained with the magnetic field aligned parallel and antiparallel to the light propagation axis to eliminate contributions from the CD background and glass strain.

X-Band EPR spectra were recorded using a Bruker ESP 300E spectrometer equipped with a Varian EIP model 625A continuous wave frequency counter. The sample temperature was maintained at 20 K by an Oxford ESR 900 continuous flow liquid He cryostat that was regulated by an Oxford ITC temperature controller. Spectra were simulated using the EasySpin program of Stoll and Schweiger.[27]

**Computations.** Initial coordinates for the whole protein quantum mechanics/molecular mechanics (QM/MM) geometry optimizations were generated as previously described.[19] In short, two published crystal structures of mouse/rat CDO [Protein Data Bank (PDB) entries 2ATF and 3ELN] were modified appropriately and used to build the initial coordinates for whole-protein WT and H155A CDO models. Importantly, the QM/MM-optimized CDO models obtained using this approach were found to agree well with a high-resolution crystal structure of Cys-bound mouse CDO that has recently been published.[14] Also, the good agreement between the experimentally derived and computationally predicted spectroscopic parameters for the different CDO species investigated (see below) indicates that the X-ray crystal structures represent the dominant protein structures in solution. Guided by a previous characterization of Cys-bound WT Fe(III)CDO, our models of both the Cys and Sec adducts of Fe(III)CDO additionally featured a hydroxide anion bound to the Fe center.[17] In preparing (H$_2$O/Cys) and (H$_2$O/Sec)-Fe(II)CDO models, we moved a water molecule from elsewhere in the QM

region to within bonding distance of the Fe center, to maintain the same total number of atoms in the QM region for the five- and six-coordinate models. To generate initial models for the H155A CDO variant, the crystal structure coordinates were manually altered by replacing the side chain of residue 155 with an alanine side chain prior to any geometry optimization step. For all optimizations, the QM/MM package as implemented in Gaussian09[28] was utilized in conjunction with Amber force field[29] parameters for MM region atoms and density functional theory (DFT) in combination with the B3LYP[30,31] functional for QM region atoms. The 6-31G[32] basis set was used for all QM atoms, with the exception of iron, all atoms immediately coordinated to it, and any exogenous water, hydroxide, nitric oxide, or dioxygen ligand, for which TZVP[33] was used instead. After a converged whole-protein structure was obtained, residues H86, H88, and H140 as well as iron and any exogenous ligands were excised and the endogenous amino acid residues were capped with methyl groups at the $\beta$ carbon with C−H bond lengths of 1.1 Å. These active site models were then used for further calculations as described below (atomic coordinates for all of these models are provided in Tables S4−S14 of the Supporting Information).

Spin-unrestricted DFT calculations were performed in Orca 2.9.1[34] using the same functional and basis sets that were used for the QM portion of the QM/MM optimization. PyMOL version 1.5.0.4[35] was utilized to generate isosurface plots of the calculated molecular orbitals (MOs) using an isodensity value of 0.05 au. Although previous attempts to utilize time-dependent DFT (TD-DFT) in conjunction with the B3LYP functional for predicting the absorption spectra of CDO species proved to be unsuccessful,[17] the TD-DFT-computed Abs spectra obtained with the CAM-B3LYP[36] functional for both the reduced and oxidized WT and H155A Cys-bound CDO active sites are qualitatively similar to those predicted with the semiempirical INDO/S-CI method (which we successfully employed in earlier studies of CDO species[17,19]), with both approaches adequately reproducing the key spectral trends observed experimentally. The TD-DFT and INDO/S-CI results were used to simulate Abs spectra by assuming that each electronic transition gives rise to a Gaussian band with a constant bandwidth (see Figures S4−S7 of the Supporting Information). Because the TD-DFT and INDO/S-CI computational results are qualitatively similar, only the former will be discussed in the text. The gOpenMol software package[37,38] with an isodensity value of 0.005 au was used to generate electron density difference maps (EDDMs) for the most intense transitions contributing to the TD-DFT-computed Abs spectra of the Cys adducts of WT Fe(II)CDO and Fe(III)CDO (see the Supporting Information for more details).

In the DFT-based calculation of EPR parameters, the coupled−perturbed self-consistent field (SCF) approach was utilized as implemented in Orca 2.9.1, using the B3LYP hybrid functional and the CP(PPP)[39,40] basis set for iron, IGLO-III[41] for the nitrogen of the NO, and TZVP[33] for the remaining atoms. All orbitals within ±100 hartree of the HOMO−LUMO gap were considered, and the origin of the **g** tensor was set at the center of the electronic charge. A high-resolution radial grid with an integration accuracy of 7.0 was used for the Fe atom and the nitrogen of the NO ligand (if present). Both spin−spin and spin−orbit contributions to the **D** tensor were considered for $S > \frac{1}{2}$ systems.

## ■ SPECTROSCOPIC RESULTS

**Cys and Sec Adducts of H155A CDO.** The Abs and MCD spectra of as-isolated WT CDO in the presence of Cys and Sec were previously published and analyzed within the framework of resonance Raman experiments and computational work.[15] Although the as-isolated protein contains a mixture of Fe(II)- and Fe(III)CDO, the Abs and MCD features exhibited by the corresponding Cys and Sec adducts occur in distinct spectral regions and can thus be probed simultaneously. Specifically, in the case of the Cys-bound CDO species, the Abs features at 32000 and 15700 cm$^{-1}$ (along with their respective MCD features) have been shown to arise from $S_{Cys} \rightarrow$ Fe(II) and $S_{Cys} \rightarrow$ Fe(III) charge transfer (CT) transitions, respectively. Similarly, the Abs and MCD features at 30000 and 13250 cm$^{-1}$ displayed by the Sec-bound CDO species were assigned as $Se_{Sec} \rightarrow$ Fe(II) and $Se_{Sec} \rightarrow$ Fe(III) CT transitions, respectively. The red-shift of the Sec-based CT features relative to their Cys-derived counterparts was attributed to a destabilization of the occupied $Se_{Sec}$-based frontier molecular orbitals with respect to their $S_{Cys}$ counterparts.[15]

As is the case for WT CDO, as-isolated H155A CDO contains a mixture of Fe(II)- and Fe(III)-bound active sites in a ratio of ∼45:55. Upon exposure of the variant to Cys, features similar to those observed in the MCD spectrum of as-isolated WT CDO appear in the H155A CDO MCD spectrum (see Figure 2). The features of the Cys-bound H155A Fe(III)CDO
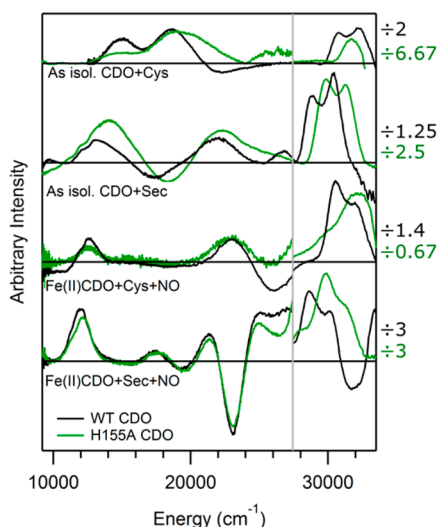


**Figure 3.** X-Band EPR spectra (at 20 K) of as-isolated WT and H155A CDO in the presence of Cys. No features that can be attributed to CDO species were observed outside the region shown. For simulation parameters, see Table S1 of the Supporting Information.

The EPR spectra obtained for as-isolated WT and H155A CDO in the presence of Cys (Figure 3) are very similar. Because only the Fe(III)CDO fraction can be observed in perpendicular-mode X-band EPR experiments, this result indicates that truncation of the H155 side chain has minimal effects on the electronic structure of the Cys-bound oxidized enzyme. Both EPR spectra in Figure 3 are characteristic of high-spin Fe(III) species with nearly rhombic symmetry (for EPR fit parameters, see Table S1 of the Supporting Information). Thus, consistent with the MCD data presented above, our EPR data indicate that the geometric and electronic structures of the Cys-bound Fe(III)CDO active site are insignificantly affected by the H155A substitution. Interestingly, however, the EPR signal of the Cys adduct of H155A Fe(III)CDO is noticeably broadened because of increased **g** strain, suggesting that the conformation of the enzyme−substrate complex is less tightly controlled in the variant.

Exposure of as-isolated H155A CDO to Sec leads to the appearance of features in the MCD spectrum consistent with direct $Se_{Sec}$ ligation to the Fe center (see Figure 2). As in the case of Cys-bound Fe(II)CDO, the MCD features associated with the reduced fraction of Sec-bound active sites undergo a substantial blue-shift in response to the H155A substitution. A small blue-shift is also observed for the features arising from the Sec-bound Fe(III)CDO fraction, even though their Cys-derived counterparts appear to be largely unaffected by the H155A substitution (*vide supra*). However, this difference presumably stems from the fact that the MCD features of Sec-bound Fe(III)CDO are considerably more intense and better resolved than those of the Cys-bound oxidized enzyme, which allows for a more precise determination of band shifts when the substrate analogue is used. Collectively, our results indicate that exposure of H155A Fe(II)CDO and Fe(III)CDO to Cys or Sec leads to the formation of enzyme−substrate complexes that are similar to, but not identical with, those of the WT enzyme, with the larger differences involving the Fe(II)-bound fraction.



**Figure 2.** MCD spectra (at 4.5 K and 7 T) of various WT (black) and H155A (green) CDO species examined in this work. Note the scale change at ∼28000 cm$^{-1}$, where the factors by which the intensities in the higher-energy region were scaled are provided on the right.

fraction (which appear at <28000 cm$^{-1}$) are only slightly shifted from their WT counterparts. In contrast, those displayed by the Cys-bound Fe(II)CDO fraction are sufficiently blue-shifted in the variant spectrum that only the lower-energy component of the pair of WT Fe(II)CDO features is observed. Despite these differences, the appearance of MCD features in the near-UV region upon exposure of H155A Fe(II)CDO to Cys provides direct evidence for the formation of an enzyme−substrate complex similar to that of the WT enzyme. This conclusion is further supported by the previous observation that H155A CDO is catalytically active, albeit at a reduced (∼100-fold) rate relative to that of the WT protein.[3]
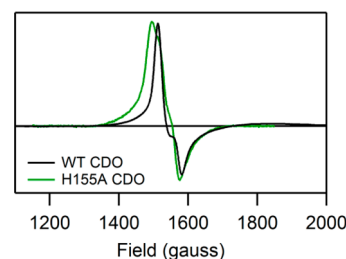
**NO Adducts of Cys- and Sec-Fe(II)CDO.** While most electronic transitions appear at higher energies for Cys- and Sec-bound H155A Fe(II)CDO than for the corresponding WT species, minimal spectral differences are observed between the corresponding NO adducts. Specifically, the new features observed upon binding of NO to Cys-bound or Sec-bound H155A Fe(II)CDO in the 10000−28000 cm$^{-1}$ range are nearly identical to those displayed by the analogous WT CDO species in terms of both their energies and relative intensities (see Figure 2, where features appearing at >28000 cm$^{-1}$ are attributed to Cys- or Sec-bound active sites that did not react with NO). Thus, on the basis of our previous Abs and MCD band assignments for the nitrosyl adducts of the WT enzyme,[19]

we can conclude that neither the donor (i.e., the Fe $3d_{xy}$-, $3d_{xz}$-, and $3d_{yz}$-based) nor the acceptor (unoccupied NO $\pi^*$-based) molecular orbitals (MOs) for these transitions are significantly affected by the H155A substitution. Consistent with this conclusion, the $g$ values and $^{14}N$ hyperfine coupling constant obtained from fits of the EPR spectra of the (NO/Cys) adducts of H155A and WT Fe(II)CDO are also extremely similar, though a slightly larger spread in $g$ is observed for the former complex (see Figure 4 for spectra and Table S2 of the
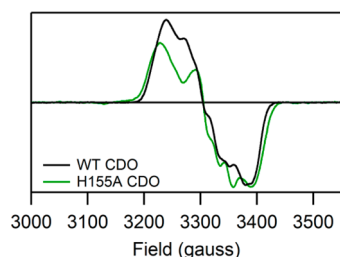


**Figure 4.** X-Band EPR spectra (at 20 K) of the (NO/Cys) adducts of H155A and WT Fe(II)CDO. No features that can be attributed to CDO species were observed outside the region shown. For simulation parameters, see Table S2 of the Supporting Information.

Supporting Information for fit parameters). Hence, the preference of the (NO/Cys) adduct of WT Fe(II)CDO to adopt an unusual $S = \frac{1}{2}$ ground state (with the single unpaired electron residing in an NO $\pi^*$-based MO that is weakly $\sigma$-bonding with the Fe center)[18] persists upon the removal of the H155 imidazole group.

**Cys- and Sec-Fe(III)CDO in the Presence of Azide.** We have previously shown that even when a large molar excess of azide is added to Cys- or Sec-bound Fe(III)-WT CDO, this $O_2^{\bullet-}$ analogue binds to only a small fraction of active sites to form an $S = \frac{1}{2}$ inner-sphere complex, which precludes a direct characterization of this complex by MCD spectroscopy.[17] The very modest shifts of the MCD features that are observed upon exposure of Cys- or Sec-bound Fe(III)-WT CDO to azide can be attributed to azide occupying a prebinding site formed in part by the guanidyl side chain of residue R60.[17] Exposing Cys- or Sec-bound H155A Fe(III)CDO to azide also results in modest MCD band shifts (Figure S3 of the Supporting Information); however, the magnitude of these shifts is greater than in the case of the WT enzyme. This finding is consistent with a less rigidly bound Cys ligand in the absence of the H155

imidazole group, which allows perturbations to the prebinding site to be relayed more effectively to the Fe center.

## ■ COMPUTATIONAL RESULTS

**General Approach.** On the basis of the spectroscopic data presented above and our previous studies of WT CDO, the following models were generated for both H155A and WT CDO via whole-protein QM/MM geometry optimizations (Figure 5): $S = 2$ (Cys)-Fe(II)CDO, $S = 2$ (H$_2$O/Cys)-Fe(II)CDO, $S = \frac{5}{2}$ (OH$^-$/Cys)-Fe(III)CDO, and $S = \frac{1}{2}$ (NO/Cys)-Fe(II)CDO, as well as the $S = 0$, $S = 1$, and $S = 2$ (O$_2$/Cys)-FeCDO adducts. With the exception of the dioxygen adducts, the analogous Sec-bound adducts were also investigated, but because the results were often similar to those obtained for the Cys adducts, only cases in which major differences were observed are discussed below. The computational models were validated on the basis of a comparison of the optimized metric parameters with X-ray crystallographic data (where available) and the calculation of relevant spectroscopic observables; namely, the energies and Abs intensities of electronic transitions as well as EPR parameters (where applicable). Relevant bond distances for the Cys-bound species considered in this work are listed in Table 1, and analogous data for the Sec-bound species are provided in Table S3 of the Supporting Information.

**Cys-Fe(II)CDO Adducts.** Previous crystallographic studies revealed that Cys-bound WT Fe(II)CDO exhibits a distorted trigonal bipyramidal geometry about the Fe center with an open coordination site trans to His86 (see Figure 1).[14,19] Because no X-ray crystallographic information about the active site coordination environment of Cys-bound H155A Fe(II)-CDO is currently available, we considered both five-coordinate models and six-coordinate models additionally featuring an exogenous water ligand for the Cys and Sec adducts of H155A Fe(II)CDO (see Table 1 and Table S3 of the Supporting Information for relevant bond lengths and angles for these models). For comparison, analogous six-coordinate Cys-bound and Sec-bound models were also generated for WT Fe(II)-CDO. However, in these cases, the water molecule that was initially placed within bonding distance of the Fe center gradually moved away during the geometry optimization to yield five-coordinate species with Fe–O$_{water}$ distances of >4 Å, consistent with the X-ray crystal structure of Cys-bound WT Fe(II)CDO (Figure 1).



Cys- and (H$_2$O/Cys)-Fe(II)-CDO

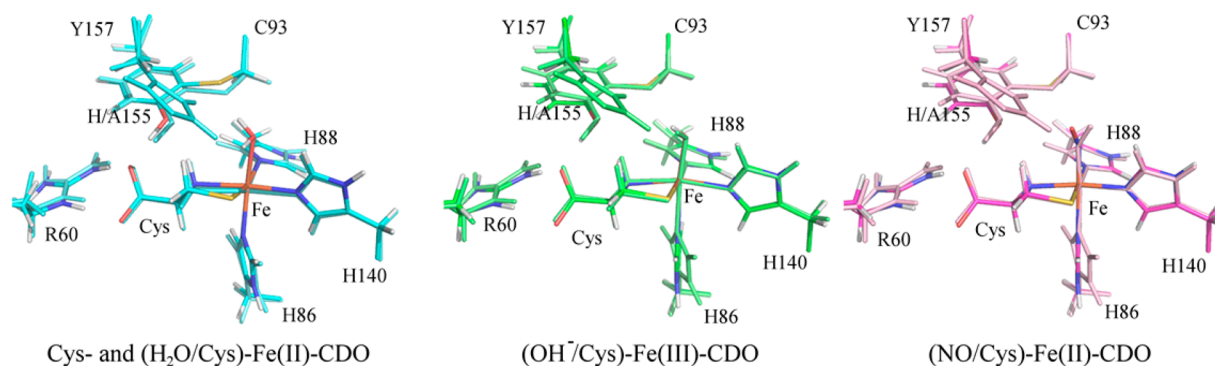(OH$^-$/Cys)-Fe(III)-CDO

(NO/Cys)-Fe(II)-CDO

**Figure 5.** Overlays of active site regions as obtained from whole-protein QM/MM optimizations, in which the models in atom-specific coloring are for H155A CDO and those with monochromatic coloring are for WT CDO. In the case of Cys-bound Fe(II) CDO, the six-coordinate H155A (H$_2$O/Cys)-Fe(II)CDO model is shown. Backbone atoms (with the exception of the $\alpha$-carbons) have been omitted for the sake of clarity.

**Table 1. Bond Distances (in angstroms) for Various Cys-Bound CDO Species As Obtained by X-ray Crystallography (PDB entry 4JTO) or Whole-Protein QM/MM Optimizations (all other models listed), in Which X Refers to the Ligating Atom of the Sixth Ligand Present at the Fe Center (where applicable)[a]**

| species | Fe−N$_{H86}$ | Fe−N$_{H88}$ | Fe−N$_{H140}$ | Fe−S$_{Cys}$ | Fe−N$_{Cys}$ | Fe−X | Cys-R60, 1 | Cys-R60, 2 | Cys-Y157 |
|---|---|---|---|---|---|---|---|---|---|
| 4JTO, WT (Cys)-Fe(II)CDO[b] | 1.893 | 2.199 | 2.110 | 2.291 | 2.262 | N/A | N/A | N/A | N/A |
| WT (Cys)-Fe(II)CDO | 2.153 | 2.184 | 2.177 | 2.368 | 2.250 | N/A | 1.800 | 2.014 | 1.537 |
| H155A (Cys)-Fe(II)CDO | 2.158 | 2.198 | 2.172 | 2.372 | 2.256 | N/A | 1.717 | 2.134 | 1.552 |
| H155A (H$_2$O/Cys)-Fe(II)CDO | 2.205 | 2.273 | 2.142 | 2.521 | 2.278 | 2.311 | 1.734 | 2.188 | 1.552 |
| WT (OH$^-$/Cys)-Fe(III)CDO | 2.326 | 2.299 | 2.111 | 2.445 | 2.223 | 1.880 | 1.984 | 1.791 | 1.532 |
| H155A (OH$^-$/Cys)-Fe(III)CDO | 2.328 | 2.287 | 2.116 | 2.428 | 2.237 | 1.872 | 2.110 | 1.717 | 1.549 |
| WT (NO/Cys)-Fe(II)CDO | 2.113 | 2.110 | 2.013 | 2.369 | 2.115 | 1.769 | 1.772 | 2.008 | 1.529 |
| H155A (NO/Cys)-Fe(II)CDO | 2.145 | 2.160 | 2.026 | 2.339 | 2.083 | 1.776 | 1.707 | 2.163 | 1.535 |

[a]For the analogous Sec-bound analogues, see Table S3 of the Supporting Information. [b]Crystal structure at 2.00 Å resolution, from ref 14.
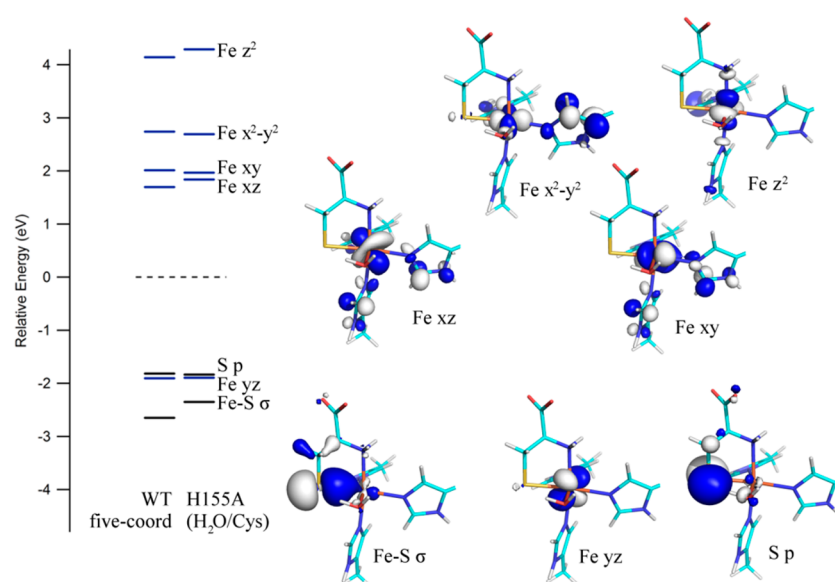


**Figure 6.** DFT-computed energies of relevant spin-down MOs for the active site models of WT Cys-Fe(II)CDO and H155A (H$_2$O/Cys)-Fe(II)CDO, along with boundary surface plots of key MOs of the H155A variant. The orbital energies for both models were adjusted such that the β-HOMO (a ligand-based orbital with essentially identical compositions for both species) lies at 0 eV. Note that the primarily water-based MOs for the H155A model are present at significantly lower energies and have been omitted from this diagram.

A comparison of the SCF energies for the QM region of the optimized whole-protein models of substrate-bound reduced H155A CDO reveals that the six-coordinate (H$_2$O/Cys)-Fe(II) complex is more stable than its five-coordinate Cys-only bound analogue by ∼39 kcal/mol (note that this value provides only a rough estimate of the binding energy and ignores any entropic contributions). Similarly, the (H$_2$O/Sec)-Fe(II) complex is favored over the five-coordinate Sec-only model by ∼51 kcal/mol.

Because Cys-bound WT Fe(II)CDO has been crystallographically shown to possess a five-coordinate Fe center,[14] the experimental Abs spectrum for this species can be compared to the TD-DFT-predicted spectrum for the QM/MM-optimized five-coordinate active site model to aid in the validation of our computational methodology. As shown in Figure S6 of the Supporting Information, the TD-DFT-computed Abs spectrum for Cys-bound WT Fe(II)CDO exhibits a pair of intense features in the range of 25000−31000 cm$^{-1}$ that arise from transitions containing primarily S$_{Cys}$ → Fe(II) CT character, in good agreement with our MCD data obtained for WT Cys-Fe(II)CDO (Figure 2). The computed Abs spectrum for the five-coordinate H155A Cys-Fe(II)CDO model can almost be superimposed on that predicted for the corresponding WT

CDO model, as expected on the basis of the highly similar active site regions of these models. In contrast, the TD-DFT-computed Abs spectrum for the six-coordinate H155A (H$_2$O/Cys)-Fe(II)CDO model is noticeably blue-shifted from the other two spectra (Figure S6 of the Supporting Information), which concurs nicely with the MCD spectral changes caused by the H155A substitution (Figure 2). For this reason, along with the fact that our QM/MM computations predict the (H$_2$O/Cys) adduct of H155A Fe(II)CDO to be more stable than the five-coordinate Cys-only adduct with the water molecule residing outside of the Fe coordination sphere (vide supra), we conclude that Cys-bound H155A Fe(II)CDO features a six-coordinate Fe center. The striking blue-shifts of the S$_{Cys}$ → Fe(II) and Se$_{Sec}$ → Fe(II) CT transitions of Cys- and Sec-bound H155A Fe(II)CDO, respectively, in response to the H155A substitution can, therefore, be attributed to the decreased Lewis acidity of the Fe(II) ion in the variant due to coordination of an additional ligand.

The most obvious difference between the five- and six-coordinate Cys-bound H155A CDO models (other than the absence of the H$_2$O ligand in the former) involves the bond angles about the Fe center, with τ parameters of 0.46 and 0.19, respectively (where τ = 1 describes a trigonal bipyramidal

geometry and $\tau = 0$ signifies octahedral or square pyramidal coordination[42]). Binding of a weakly donating water ligand to the Fe center also causes the Fe–S$_{Cys}$ bond and the Fe–N$_{H88}$ bond trans to it to lengthen substantially (by 0.15 and 0.08 Å, respectively). The other Fe–ligand bond distances change by <0.05 Å upon water binding, and the hydrogen bonding interactions between the Cys substrate carboxylate group and residues Y157 and R60 are largely unperturbed. In contrast, the atoms of the Cys portion of the C93–Y157 cross-link move quite substantially in response to the binding of water to the active site. In the WT CDO model, the phenolic oxygen is situated to engage in a hydrogen bonding interaction with H155 (O···H distance of 2.26 Å) and the S and C$\beta$ atoms of C93 are nearly coplanar with the phenol ring of Y157 (out-of-plane displacements of 0.03 and 0.06 Å, respectively, where the tyrosine ring plane is defined by the positions of the two C$\delta$ atoms and C$\zeta$). In the absence of the H155 side chain (and thus the presence of both Cys and water at the Fe center), the atoms of the cross-link are reoriented, with the S and C$\beta$ atoms of C93 moving to ∼0.35 and ∼0.17 Å above the Y157 ring plane, respectively. This permits the formation of a relatively short (2.20 Å) hydrogen bond between the sulfur of C93 and a hydrogen on the water ligand that is absent in the WT Cys-Fe(II) CDO model. However, despite this distortion of the cross-link in the variant, the hydrogen bond distance between Y157 and the substrate Cys is similar to that in WT CDO, because of the ability of the phenolic hydrogen to rotate out of the ring plane. Very similar geometric trends (including hydrogen bond distances and cross-link planarity) are predicted to exist between the WT Sec-Fe(II)CDO and H155A (H$_2$O/Sec)-Fe(II)CDO models.

Despite the different coordination number adopted by the iron atom in the active site models of the catalytically relevant WT Cys-Fe(II)CDO and H155A (H$_2$O/Cys)-Fe(II)CDO species, the DFT-computed electronic structures for these models show only modest differences. Both species are predicted to possess a high-spin Fe(II) center, as all five Fe 3d-based spin-up ($\alpha$) molecular orbitals (MOs) are occupied, while only one of the Fe 3d-based spin-down ($\beta$) MOs is occupied (see Figure 6). Although in the H155A Cys-Fe(II)CDO model a water molecule occupies the open coordination site that is present in the WT model, the relative energies of the unoccupied Fe 3d-based $\beta$-MOs exhibit relatively small differences. Note, however, that a direct comparison of these MO energies is complicated by the fact that numerous unoccupied $\beta$-MOs contain significant Fe 3d orbital character.

Although the five-coordinate H155A Cys-Fe(II)CDO active site model is predicted to be less stable than the corresponding six-coordinate adduct, a comparison of the five-coordinate WT and H155A Cys-Fe(II)CDO models provides clues about how the WT enzyme retains an open coordination site for O$_2$ binding in the Cys-bound form. Both of these models converged to very similar geometries, with Fe–ligand bond lengths in close agreement with those observed in a recently published crystal structure (see Table 1).[14] The coordination site trans to H86 is clearly open, with the Cys sulfur, Fe center, and nitrogen of H88 forming a "bite angle" of 143.5° for both species. Three hydrogen bonding interactions between the protein matrix and the carboxylic acid group of the substrate Cys are found in both active site models; namely, two with the guanidyl group of R60 and one with the phenol of Y157. Experimental support for the existence of such stabilizing interactions with the Cys substrate carboxylate is provided by the fact that the relative positioning of the H-bond-donating residues R60 and Y157 is similar in our optimized models and the WT CDO crystal structure. One of the most notable differences between the five-coordinate WT and H155A Cys-Fe(II)CDO models involves the relative positions of the atoms in the C–Y cross-link. In the WT model, both the S$_{Cys}$ and C$\beta_{Cys}$ atoms are essentially coplanar with the atoms of the Y157 ring. In contrast, in the five-coordinate H155A Cys-Fe(II)CDO model, the sulfur atom is displaced from this plane by 0.28 Å, allowing more room for water to bind to the Fe center without steric clashes.

**(OH⁻/Cys)-Fe(III)CDO Adducts.** In a recent spectroscopic and computational study, we concluded that the Cys adduct of WT Fe(III)CDO additionally features a hydroxide ligand to complete a distorted octahedral coordination environment at the Fe(III) center.[17] For this reason, an analogous adduct was generated computationally for the H155A variant via whole-protein QM/MM geometry optimization. As shown in Table 1 and Figure 5, the H155A and WT (OH⁻/Cys)-Fe(III)CDO active site models exhibit only minor geometric differences. The Fe–ligand bond lengths are nearly identical in the two models, while one of the two R60···Cys hydrogen bond distances is lengthened by 0.13 Å in response to the H155A substitution. This suggests the Cys substrate is granted slightly greater conformational freedom in the H155A (OH⁻/Cys)-Fe(III)CDO complex, consistent with the increased $g$ strain observed in the EPR spectrum of this species (*vide supra*). Additionally, as in the case of the Cys-bound Fe(II)CDO species, the relative positioning of the C93–Y157 cross-link differs between the (OH⁻/Cys) adducts of WT and H155A Fe(III)CDO, with the S$_{Cys}$ and C$\beta$ atoms being displaced from the Tyr ring plane by 0.50 and 0.50 Å, respectively, in the WT model and by 0.14 and 0.23 Å, respectively, in the H155A model. While in the reduced state the driving force for distorting the C–Y cross-link in the variant is the formation of a hydrogen bond to the coordinated water (*vide supra*), neither of the (OH⁻/Cys)-Fe(III)CDO models features a hydrogen bond donor to the hydroxide ligand. Instead, in the oxidized state, the magnitude of the displacement of the S$_{Cys}$ and C$\beta$ atoms from the Tyr ring plane is largely dictated by the strength of the H-bonding interaction between the phenolic oxygen of Y157 and residue 155. As no such H-bond is present in the H155A variant, the Y157 ring can adopt a less strained conformation, yielding bond angles more consistent with sp² hybridization.

The computed electronic structures for the (OH⁻/Cys)-Fe(III)CDO active site models are only weakly affected by the geometric differences caused by the H155A substitution (see Figure S8 of the Supporting Information), as required experimentally by our MCD and EPR data (see Figures 2 and 3). However, the highest occupied molecular orbital (HOMO) and HOMO−1 are slightly stabilized in energy in the variant, while the energies of the Fe 3d-based $\beta$-MOs are essentially unperturbed. As a result, the energy differences between the donor and acceptor orbitals for the key electronic transitions are expected to increase slightly from the WT to the H155A (OH⁻/Cys)-Fe(III)CDO adducts, which is consistent with our MCD data (Figure 2) and TD-DFT-predicted Abs spectra (Figure S7 of the Supporting Information).

**(NO/Cys)-Fe(II)CDO Adducts.** The geometries of the computationally derived models for the (NO/Cys)-adducts of WT and H155A Fe(II)CDO are quite similar, with the only
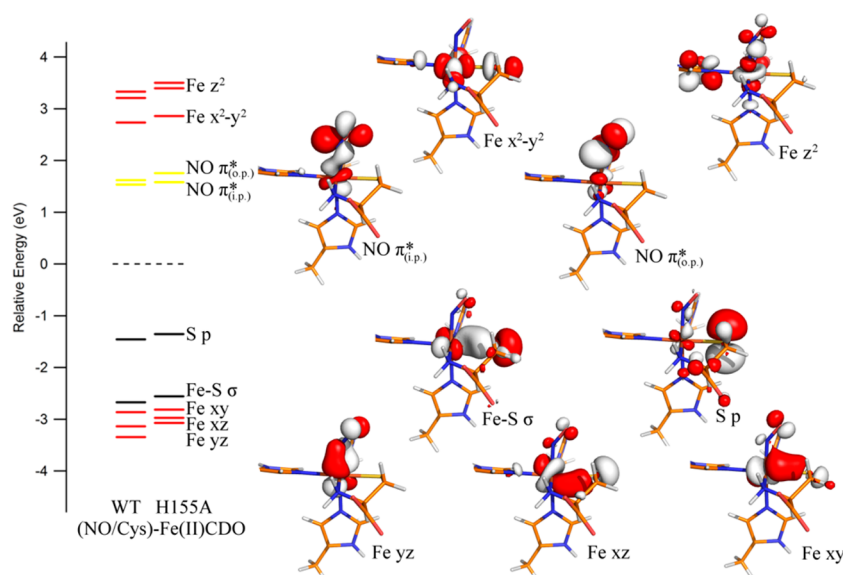
**Figure 7.** DFT-computed energies of relevant spin-down MOs for the active site models of WT and H155A (NO/Cys)-Fe(II)CDO, along with boundary surface plots of key MOs of the H155A species. The orbital energies for both models were adjusted such that the $\beta$-HOMO (a ligand-based orbital with essentially identical compositions for both species) lies at 0 eV.

major differences concerning the two hydrogen bonds between the Cys carboxylic acid and the R60 guanidyl group (which change by +0.07 and −0.16 Å from WT to H155A CDO) and the relative positioning of the $S_{Cys}$ and $C\beta_{Cys}$ cross-link atoms (which are much less displaced from the Tyr plane in the variant). Additionally, the bond angle formed among the nitrogen of the NO ligand, Fe, and the nitrogen of the His ligand trans to the NO binding site increases slightly from 171° to 176° in the H155A model. The orientation of the NO ligand also differs between the two models, though the lack of hydrogen bonds involving this ligand suggests that changes in the $S_{Cys}$−Fe−N−O dihedral angle come at a small energetic penalty.

Despite the larger differences in the active site geometries of the (NO/Cys)-Fe(II)CDO adducts as compared to the (OH⁻/Cys)-Fe(III)CDO adducts of the WT and H155A enzymes, the computed electronic structures for the nitrosyl adducts are very similar (Figure 7), consistent with our MCD and EPR data (Figures 2 and 4, respectively). In particular, the composition of the formally singly occupied molecular orbital (SOMO), which corresponds to the filled counterpart of the in-plane (i.p.) NO $\pi^*$-based $\beta$-MO oriented in the Fe−N−O plane, is essentially identical for the WT and H155A (NO/Cys)-Fe(II)CDO species, as stipulated by their highly similar EPR spectra. Although the $\beta$-MOs of the H155A (Cys/NO)-Fe(II)CDO adduct are slightly destabilized in energy relative to their WT counterparts, all orbitals undergo a relatively uniform shift such that the energetic differences between the donor and acceptor orbitals for the electronic transitions responsible for the dominant MCD features remain essentially unchanged. Nonetheless, minor differences in the relative magnitudes of the Fe−NO $\sigma$- and $\pi$-bonding interactions between WT and H155A (Cys/NO)-Fe(II)CDO do exist, as revealed by the slightly larger energetic splitting between the unoccupied NO $\pi^*$-based $\beta$-MOs in the variant.

## DISCUSSION

The role of the C93−Y157 cross-link in CDO has puzzled researchers since its identification in the first X-ray crystal

structure of the enzyme.[13] From a recent EPR investigation of the (CN⁻/Cys)-Fe(III)CDO adducts of as-isolated and fully cross-linked WT enzyme, it was suggested that the phenol group of Y157 engages in a hydrogen bonding interaction with the substrate Cys carboxylic acid that is key for the proper positioning of the latter.[3] Additionally, the sulfur of C93 could provide steric bulk to the active site pocket, potentially modulating the orientation in which any exogenous sixth ligand (including $O_2$) binds to the Fe center.[3] The phenol of Y157 is both a hydrogen bond donor to the substrate and a hydrogen bond acceptor from the H155 imidazole ring, so its position within the active site pocket is carefully adjusted. On the basis of the results obtained in this study, we suggest an additional role for H155 in tuning the relative positioning of the C−Y cross-link within the active site pocket. In the absence of the H155 imidazole side chain, the cysteine portion of the C−Y cross-link is substantially more coplanar with the Tyr ring, except in the catalytically active, Cys-bound Fe(II)CDO species where the opposite is the case.

It is intriguing that the WT Cys-Fe(II)CDO adduct is a five-coordinate species with an open coordination site for $O_2$ binding, whereas the H155A variant appears to retain one of the originally bound water ligands upon Cys binding to form an octahedrally coordinated Fe(II) complex. Although the removal of the H155 side chain may seem to be a fairly modest perturbation, the absence of this polar side chain allows neighboring residues to reorient within the active site pocket. The binding of an additional ligand to the five-coordinate Fe(II) center requires the equatorial His−Fe−His bond angle to contract by ~10°, forcing the Fe atom to move ~0.5 Å closer to the atoms of the C93−Y157 cross-link. In WT CDO, the cross-link atoms are locked in place through H-bonding interactions with the H155 side chain, which effectively precludes water from binding to the Fe center. Alternatively, in the H155A CDO variant, the cross-link atoms are sufficiently free to move to accommodate the structural changes required for binding of water to the active site. Thus, the interplay among the H155, Y157, and C93 side chains appears to play a

key role in controlling the coordination environment about the Fe(II) center.

The preference of WT Fe(II)CDO to form a five-coordinate Cys adduct has obvious implications for the catalytic mechanism employed by this enzyme. As the Fe(II) center retains an open coordination site upon Cys coordination, dioxygen can enter the first coordination sphere without having to displace another ligand. Additionally, the binding of $O_2$ to the active site prompts the movement of the Fe center away from the H155 residue side chain, relieving any steric clashes that might otherwise have been present. Alternatively, in the case of Cys-bound H155A Fe(II)CDO, a ligand displacement is required to permit binding of $O_2$ to the Fe atom, which may help explain the lower catalytic activity displayed by this enzyme variant. To evaluate this possibility, the relative $O_2$ binding affinities of WT and H155A Fe(II)CDO were estimated from the difference in SCF energies between the Cys-bound and ($O_2$/Cys)-bound Fe(II)CDO models (note that because the enzyme models for the WT and variant enzymes contain differing numbers of atoms, a comparison of their absolute energies is meaningless). We have previously evaluated the energies for three spin states of WT ($O_2$/Cys)-Fe(II)CDO and proposed that this species has a quintet ground state [due to ferromagnetic coupling between an intermediate spin Fe(III) ion and a superoxo-based radical], with a computed energy ~9 kcal/mol lower than that of the five-coordinate Cys-bound complex and free $^3O_2$.[19] The results obtained from analogous computations for the initial $O_2$-bound intermediate of Cys-bound H155A Fe(II)CDO are compared to those reported for the WT enzyme in Figure 8.
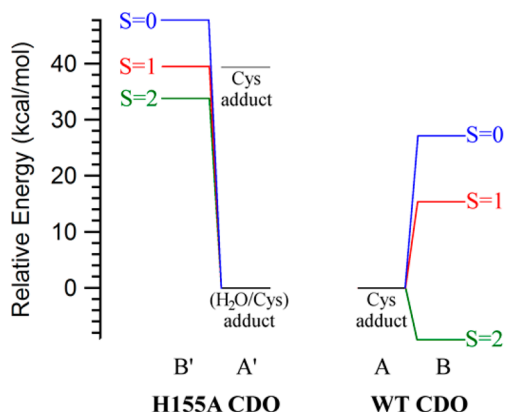


**Figure 8.** Reaction coordinate diagrams showing the computed relative energies of the Cys- and ($O_2$/Cys)-bound species (A/A′ and B/B′, respectively) of WT and H155A Fe(II)CDO. To facilitate a direct comparison between different species, the energy of the most stable Cys-bound Fe(II)CDO adduct and free $^3O_2$ was set to 0 kcal/mol in each case. For H155A CDO, the relative energies of both the five-coordinate Cys and the six-coordinate (Cys/$H_2O$) adducts are shown (gray and black, respectively). Values for the WT CDO species were taken from ref 19.

All three spin states for the six-coordinate H155A ($O_2$/Cys)-Fe(II)CDO adduct investigated in this work are significantly closer in energy to the five-coordinate than the six-coordinate Cys-bound model and free $^3O_2$ (see Figure 8). Because the six-coordinate H155A ($H_2O$/Cys)-Fe(II)CDO adduct is predicted to be stabilized over the five-coordinate Cys adduct by ~39 kcal/mol, a large energetic penalty is therefore predicted for the binding of $O_2$ to the ($H_2O$/Cys)-bound active site of H155A

Fe(II)CDO (~34 kcal/mol for the $^5$A′ to $^5$B′ pathway). Although our approach ignores entropic contributions to the free energy of $O_2$ binding, which would lower the energy of the ($O_2$/Cys) adduct for H155A CDO relative to that of the WT complex due to the release of the water molecule originally bound to the Fe(II) ion in the variant, these contributions are unlikely to compensate for the large energetic penalty associated with the $^5$A′ to $^5$B′ conversion. Hence, we propose that the drastically reduced enzymatic activity of the H155A variant (<2% of WT)[3] is due, at least in part, to a largely reduced $O_2$ binding affinity of the corresponding Cys-Fe(II)CDO adduct.

Although the ($O_2$/Cys) adducts for both WT and H155A Fe(II)CDO are predicted to possess a quintet ground state ($^5$B and $^5$B′, respectively), the electron configuration differs between the two models. The WT species has previously been shown to be best described as an intermediate spin Fe(III) ion coupled ferromagnetically to a superoxide-based radical.[19] Alternatively, the computed electronic structure for the ($O_2$/Cys) adduct of H155A Fe(II)CDO is more consistent with a high-spin Fe(II) ion bound to a singlet dioxygen moiety. This distinct electron distribution probably reflects the unusual binding mode adopted by the dioxygen moiety in this species, which was found to be end-on to the Fe−S bond even if the $O_2$ moiety was initially placed within bonding distance of the Fe(II) atom prior to the QM/MM geometry optimization. A similar configuration of substrate $O_2$ was previously seen in a crystal structure of WT CDO in the presence of Cys and air (PDB entry 3ELN),[43] though it was later found that this species does not represent a true reaction intermediate.[44] It is important to note that even though the unusual $O_2$ binding mode may contribute to the high relative energy of the $^5$B′ intermediate, the relative energies of the $^1$B′ and $^3$B′ species are also ~25 kcal/mol higher than those of their structurally nearly identical WT counterparts ($^1$B and $^3$B, respectively).

## ■ CONCLUSIONS

Although the presence of the H155 side chain appears to have modest to no effects on the geometric and electronic structures of the CDO active site in some states, a drastic difference is seen for the catalytically relevant Cys-bound Fe(II) center. In the presence of the H155 side chain (i.e., in WT CDO), X-ray crystallographic and computational results indicate that the Cys-bound WT Fe(II)CDO active site adopts a distorted trigonal bipyramidal coordination geometry, which allows the reaction with $O_2$ to proceed with a low activation energy barrier, and thus a relatively fast rate (the overall rate constant for Cys oxidation by CDO is 8.6 s$^{-1}$). Remarkably, the introduction of a third-sphere amino acid substitution to generate the H155A CDO variant causes a decrease in the turnover rate of almost 2 orders of magnitude. While the molecular basis for this drastic reduction in the overall rate constant for Cys oxidation was previously unknown, the spectroscopic and computational data obtained in this study lead us to propose that a six-coordinate ($H_2O$/Cys)-Fe(II)-CDO complex is formed in the variant because of the ability of the cross-link to accept a hydrogen bond from the coordinated $H_2O$ molecule in the absence of the H155 side chain. Thus, for $O_2$ binding to this complex to occur, the coordinated water molecule must first be removed to form a transient five-coordinate Fe(II) species (likely in an entropically controlled process that depresses the rate at which $O_2$ binding proceeds). The H155 side chain thus appears to assume a key role in the

CDO catalytic cycle by discouraging the binding of a water molecule in the position where $O_2$ must bind to the Cys-bound Fe(II)CDO complex to initiate catalysis. Because in the non-cross-linked WT enzyme the S atom of the C93 side chain is granted even more conformational freedom than in the H155A CDO variant, it is tempting to speculate that the binding of a water molecule to the Cys-bound Fe(II)CDO complex is also responsible for the low catalytic activity of CDO lacking the cross-link. In this scenario, replacement of C93 with a residue that is unable to serve as a hydrogen bond acceptor and thus to stabilize coordinated solvent should restore full activity, consistent with the results that have recently been reported for C93G CDO.[45]

## ASSOCIATED CONTENT

### Ⓢ Supporting Information

Thin-layer chromatogram confirming the enzymatic activity of the H155A CDO variant, SDS−PAGE gel illustrating sample purity, comparison of experimentally derived and computationally predicted EPR parameters, MCD spectra of substrate (analogue)-bound CDO in the presence of azide, comparison of structural parameters of various QM/MM-optimized active site models of Sec-bound CDO species, INDO/S-CI- and TD-DFT-predicted Abs spectra, and Cartesian coordinates for QM/MM-optimized active sites. The Supporting Information is available free of charge on the ACS Publications website at DOI: 10.1021/acs.biochem.5b00171.

## AUTHOR INFORMATION

### Corresponding Author

*Address: 1101 University Ave., Madison, WI 53706. E-mail: brunold@chem.wisc.edu. Phone: (608) 265-9056. Fax: (608) 262-6143.

### Present Address

§E.J.B.: Department of Chemistry, The Pennsylvania State University, University Park, PA 16802.

### Notes

The authors declare no competing financial interest.

## ACKNOWLEDGMENTS

## ABBREVIATIONS

CDO, cysteine dioxygenase; Cys, cysteine; Sec, selenocysteine; EPR, electron paramagnetic resonance; MCD, magnetic circular dichroism; Abs, electronic absorption; DFT, density functional theory; TD-DFT, time-dependent density functional theory; RT, room temperature; LT, low temperature; QM/MM, quantum mechanics/molecular mechanics; MO, molecular orbital; EDDM, electron density difference map; SCF, self-consistent field; INDO/S-CI, intermediate neglect of differential overlap/singles-configuration interaction; HOMO, highest occupied molecular orbital; LUMO, lowest unoccupied molecular orbital.

## REFERENCES

(1) Yamaguchi, K., and Hosokawa, Y. (1987) Cysteine Dioxygenase. *Methods Enzymol.* 143, 395−403.

(2) Lombardini, J. B., Singer, T. P., and Boyer, P. D. (1969) Cysteine Oxygenase. 2. Studies on Mechanism of Reaction with [18]Oxygen. *J. Biol. Chem.* 244, 1172−1175.

(3) Li, W., Blaesi, E. J., Pecore, M. D., Crowell, J. K., and Pierce, B. S. (2013) Second-Sphere Interactions between the C93−Y157 Cross-Link and the Substrate-Bound Fe Site Influence the $O_2$ Coupling Efficiency in Mouse Cysteine Dioxygenase. *Biochemistry* 52, 9104−9119.

(4) Stipanuk, M. H., and Ueki, I. (2011) Dealing with methionine/homocysteine sulfur: Cysteine metabolism to taurine and inorganic sulfur. *J. Inherited Metab. Dis.* 34, 17−32.

(5) Ueki, I., Roman, H. B., Valli, A., Fieselmann, K., Lam, J., Peters, R., Hirschberger, L. L., and Stipanuk, M. H. (2011) Knockout of the Murine Cysteine Dioxygenase Gene Results in Severe Impairment in Ability to Synthesize Taurine and an Increased Catabolism of Cysteine to Hydrogen Sulfide. *Am. J. Physiol.* 301, E668−E684.

(6) Slivka, A., and Cohen, G. (1993) Brain Ischemia Markedly Elevates Levels of the Neurotoxic Amino-acid, Cysteine. *Brain Res.* 608, 33−37.

(7) Pean, A. R., Parsons, R. B., Waring, R. H., Williams, A. C., and Ramsden, D. B. (1995) Toxicity of Sulfur-Containing-Compounds to Neuronal Cell-Lines. *J. Neurol. Sci.* 129, 107−108.

(8) Heafield, M. T., Fearn, S., Steventon, G. B., Waring, R. H., Williams, A. C., and Sturman, S. G. (1990) Plasma Cysteine and Sulphate Levels in Patients with Motor Neurone, Parkinson's and Alzheimer's Disease. *Neurosci. Lett.* 110, 216−220.

(9) Gordon, C., Bradley, H., Waring, R. H., and Emery, P. (1992) Abnormal Sulfur Oxidation in Systemic Lupus-Erythematosus. *Lancet* 339, 25−26.

(10) Emery, P., Bradley, H., Gough, A., Arthur, V., Jubb, R., and Waring, R. (1992) Increased prevalence of poor sulphoxidation in patients with rheumatoid arthritis: Effect of changes in the acute phase response and second line drug treatment. *Ann. Rheum. Dis.* 51, 318−320.

(11) Brait, M., Ling, S. Z., Nagpal, J. K., Chang, X. F., Park, H. L., Lee, J., Okamura, J., Yamashita, K., Sidransky, D., and Kim, M. S. (2012) Cysteine Dioxygenase 1 Is a Tumor Suppressor Gene Silenced by Promoter Methylation in Multiple Human Cancers. *PLoS One* 7, e44951.

(12) Jeschke, J., O'Hagan, H. M., Zhang, W., Vatapalli, R., Calmon, M. F., Danilova, L., Nelkenbrecher, C., Van Neste, L., Bijsmans, I., Van Engeland, M., Gabrielson, E., Schuebel, K. E., Winterpacht, A., Baylin, S. B., Herman, J. G., and Ahuja, N. (2013) Frequent Inactivation of Cysteine Dioxygenase Type 1 Contributes to Survival of Breast Cancer Cells and Resistance to Anthracyclines. *Clin. Cancer Res.* 19, 3201−3211.

(13) McCoy, J. G., Bailey, L. J., Bitto, E., Bingman, C. A., Aceti, D. J., Fox, B. G., and Phillips, G. N. (2006) Structure and Mechanism of Mouse Cysteine Dioxygenase. *Proc. Natl. Acad. Sci. U.S.A.* 103, 3084−3089.

(14) Driggers, C. M., Cooley, R. B., Sankaran, B., Hirschberger, L. L., Stipanuk, M. H., and Karplus, P. A. (2013) Cysteine Dioxygenase Structures from pH 4 to 9: Consistent Cys-Persulfenate Formation at Intermediate pH and a Cys-Bound Enzyme at Higher pH. *J. Mol. Biol.* 425, 3121−3136.

(15) Gardner, J. D., Pierce, B. S., Fox, B. G., and Brunold, T. C. (2010) Spectroscopic and Computational Characterization of Substrate-Bound Mouse Cysteine Dioxygenase: Nature of the Ferrous and Ferric Cysteine Adducts and Mechanistic Implications. *Biochemistry* 49, 6033−6041.

(16) Ye, S., Wu, X. A., Wei, L., Tang, D., Sun, P., Bartlam, M., and Rao, Z. (2007) An Insight into the Mechanism of Human Cysteine Dioxygenase: Key Roles of the Thioether-Bonded Tyrosine-Cysteine Cofactor. *J. Biol. Chem.* 282, 3391−3402.

(17) Blaesi, E. J., Fox, B. G., and Brunold, T. C. (2014) Spectroscopic and Computational Investigation of Iron(III) Cysteine Dioxygenase:

Implications for the Nature of the Putative Superoxo-Fe(III) Intermediate. *Biochemistry 53*, 5759−5770.

(18) Pierce, B. S., Gardner, J. D., Bailey, L. J., Brunold, T. C., and Fox, B. G. (2007) Characterization of the nitrosyl adduct of substrate-bound mouse cysteine dioxygenase by electron paramagnetic resonance: Electronic structure of the active site and mechanistic implications. *Biochemistry 46*, 8569−8578.

(19) Blaesi, E. J., Gardner, J. D., Fox, B. G., and Brunold, T. C. (2013) Spectroscopic and Computational Characterization of the NO Adduct of Substrate-Bound Fe(II) Cysteine Dioxygenase: Insights into the Mechanism of $O_2$ Activation. *Biochemistry 52*, 6040−6051.

(20) Crawford, J. A., Li, W., and Pierce, B. S. (2011) Single Turnover of Substrate-Bound Ferric Cysteine Dioxygenase with Superoxide Anion: Enzymatic Reactivation, Product Formation, and a Transient Intermediate. *Biochemistry 50*, 10241−10253.

(21) Dominy, J. E., Hwang, J., Guo, S., Hirschberger, L. L., Zhang, S., and Stipanuk, M. H. (2008) Synthesis of Amino Acid Cofactor in Cysteine Dioxygenase is Regulated by Substrate and Represents a Novel Post-Translational Regulation of Activity. *J. Biol. Chem. 283*, 12188−12201.

(22) Dominy, J. E., Simmons, C. R., Karplus, P. A., Gehring, A. M., and Stipanuk, M. H. (2006) Identification and characterization of bacterial cysteine dioxygenases: A new route of cysteine degradation for eubacteria. *J. Bacteriol. 188*, 5561−5569.

(23) Crowell, J. K., Li, W., and Pierce, B. S. (2014) Oxidative uncoupling in cysteine dioxygenase is gated by a proton-sensitive intermediate. *Biochemistry 53*, 7541−7548.

(24) Kleffmann, T., Jongkees, S. A. K., Fairweather, G., Wilbanks, S. M., and Jameson, G. N. L. (2009) Mass-spectrometric characterization of two posttranslational modifications of cysteine dioxygenase. *JBIC, J. Biol. Inorg. Chem. 14*, 913−921.

(25) Siakkou, E., Rutledge, M. T., Wilbanks, S. M., and Jameson, G. N. L. (2011) Correlating crosslink formation with enzymatic activity in cysteine dioxygenase. *Biochim. Biophys. Acta 1814*, 2003−2009.

(26) Fischer, D. S., and Price, D. S. (1964) A Simple Serum Iron Method Using the New Sensitive Chromogen Tripyridyl-s-triazine. *Clin. Chem. 10*, 21−31.

(27) Stoll, S., and Schweiger, A. (2006) EasySpin, a comprehensive software package for spectral simulation and analysis in EPR. *J. Magn. Reson. 178*, 42−55.

(28) Frisch, M. J., Trucks, G. W., Schlegel, H. B., Scuseria, G. E., Robb, M. A., Cheeseman, J. R., Scalmani, G., Barone, V., Mennucci, B., Petersson, G. A., Nakatsuji, H., Caricato, M., Li, X., Hratchian, H. P., Izmaylov, A. F., Bloino, J., Zheng, G., Sonnenberg, J. L., Hada, M., Ehara, M., Toyota, K., Fukuda, R., Hasegawa, J., Ishida, M., Nakajima, T., Honda, Y., Kitao, O., Nakai, H., Vreven, T., Montgomery, J. A., Jr., Peralta, J. E., Ogliaro, F., Bearpark, M., Heyd, J. J., Brothers, E., Kudin, K. N., Staroverov, V. N., Keith, T., Kobayashi, R., Normand, J., Raghavachari, K., Rendell, A., Burant, J. C., Iyengar, S. S., Tomasi, J., Cossi, M., Rega, N., Millam, J. M., Klene, M., Knox, J. E., Cross, J. B., Bakken, V., Adamo, C., Jaramillo, J., Gomperts, R., Stratmann, R. E., Yazyev, O., Austin, A. J., Cammi, R., Pomelli, C., Ochterski, J. W., Martin, R. L., Morokuma, K., Zakrzewski, V. G., Voth, G. A., Salvador, P., Dannenberg, J. J., Dapprich, S., Daniels, A. D., Farkas, O., Foresman, J. B., Ortiz, J. V., Cioslowski, J., and Fox, D. J. (2010) *Gaussian 09*, revision C.01, Gaussian, Inc., Wallingford, CT.

(29) Cornell, W. D., Cieplak, P., Bayly, C. I., Gould, I. R., Merz, K. M., Ferguson, D. M., Spellmeyer, D. C., Fox, T., Caldwell, J. W., and Kollman, P. A. (1995) A 2nd Generation Force-Field for the Simulation of Proteins, Nucleic-Acids, and Organic-Molecules. *J. Am. Chem. Soc. 117*, 5179−5197.

(30) Lee, C. T., Yang, W. T., and Parr, R. G. (1988) Development of the Colle-Salvetti Correlation-Energy Formula into a Functional of the Electron-Density. *Phys. Rev. B 37*, 785−789.

(31) Becke, A. D. (1993) Density-Functional Thermochemistry. 3. The Role of Exact Exchange. *J. Chem. Phys. 98*, 5648−5652.

(32) Hehre, W. J., Ditchfie, R., and Pople, J. A. (1972) Self-Consistent Molecular-Orbital Methods. 12. Further Extensions of Gaussian-Type Basis Sets for Use in Molecular-Orbital Studies of Organic-Molecules. *J. Chem. Phys. 56*, 2257−2261.

(33) Schafer, A., Horn, H., and Ahlrichs, R. (1992) Fully Optimized Contracted Gaussian-Basis Sets for Atoms Li to Kr. *J. Chem. Phys. 97*, 2571−2577.

(34) Neese, F. (2012) *Orca, 2.9.1, An Ab Initio, DFT and Semiempirical Electronic Structure Package.*

(35) *The PyMOL Molecular Graphics System*, version 1.5.0.4 (2012) Schrodinger, LLC, Portland, OR.

(36) Yanai, T., Tew, D. P., and Handy, N. C. (2004) A new hybrid exchange−correlation functional using the Coulomb-attenuating method (CAM-B3LYP). *Chem. Phys. Lett. 293*, 51−57.

(37) Bergman, D. L., Laaksonen, L., and Laaksonen, A. (1997) Visualization of solvation structures in liquid mixtures. *J. Mol. Graphics Modell. 15*, 301−306.

(38) Laaksonen, L. (1992) A Graphics Program for the Analysis and Display of Molecular-Dynamics Trajectories. *J. Mol. Graphics 10*, 33−34.

(39) Neese, F. (2002) Prediction and interpretation of the Fe-57 isomer shift in Mossbauer spectra by density functional theory. *Inorg. Chim. Acta 337*, 181−192.

(40) Wachters, A. J. (1970) Gaussian Basis Set For Molecular Wavefunctions Containing Third-Row Atoms. *J. Chem. Phys. 52*, 1033−1036.

(41) Kutzelnigg, W., Fleischer, U., and Schindler, M., Eds. (1990) *The IGLO method: Ab initio calculation and interpretation of NMR chemical shifts and magnetic susceptibilities*, Vol. 23, Springer-Verlag, Heidelberg. Germany.

(42) Addison, A. W., Rao, T. N., Reedijk, J., Vanrijn, J., and Verschoor, G. C. (1984) Synthesis, Structure, and Spectroscopic Properties of Copper(II) Compounds Containing Nitrogen Sulfur Donor Ligands: The Crystal and Molecular-Structure of Aqua 1,7-Bis(N-methylbenzimidazol-2′-yl)-2,6-Dithiaheptane Copper(II) Perchlorate. *J. Chem. Soc., Dalton Trans.*, 1349−1356.

(43) Simmons, C. R., Krishnamoorthy, K., Granett, S. L., Schuller, D. J., Dominy, J. E., Begley, T. P., Stipanuk, M. H., and Karplus, P. A. (2008) A Putative $Fe^{2+}$-Bound Persulfenate Intermediate in Cysteine Dioxygenase. *Biochemistry 47*, 11390−11392.

(44) Souness, R. J., Kleffmann, T., Tchesnokov, E. P., Wilbanks, S. M., Jameson, G. B., and Jameson, G. N. L. (2013) Mechanistic Implications of Persulfenate and Persulfide Binding in the Active Site of Cysteine Dioxygenase. *Biochemistry 52*, 7606−7617.

(45) Davies, C. G., Fellner, M., Tchesnokov, E. P., Wilbanks, S. M., and Jameson, G. N. L. (2014) The Cys-Tyr Cross-Link of Cysteine Dioxygenase Changes the Optimal pH of the Reaction without a Structural Change. *Biochemistry 53*, 7961−7968.